Distribution Agreement

In presenting this thesis as a partial fulfillment of the requirements for a degree from Emory University, I hereby grant to Emory University and its agents the non-exclusive license to archive, make accessible, and display my thesis in whole or in part in all forms of media, now or hereafter now, including display on the World Wide Web. I understand that I may select some access restrictions as part of the online submission of this thesis. I retain all ownership rights to the copyright of the thesis. I also retain the right to use in future works (such as articles or books) all or part of this thesis.

Yijun Dong April 16, 2018

Crystals and Liquids in Gravitationally Confined Quasi-2-Dimensional Colloidal Systems

by

Yijun Dong

Eric Weeks

Advisor

Department of Physics

Eric Weeks

Advisor

Effrosyni Seitaridou

Committee Member

James Kindt

Committee Member

2018

Crystals and Liquids in Gravitationally Confined Quasi-2-Dimensional Colloidal Systems

by

Yijun Dong

Eric Weeks

Advisor

An abstract of
a thesis submitted to the Faculty of Emory College of Arts and Sciences
of Emory University in partial fulfillment
of the requirements of the degree of
Bachelor of Sciences with Honors

Department of Physics

2018

Abstract

Crystals and Liquids in Gravitationally Confined Quasi-2-Dimensional Colloidal Systems

by Yijun Dong

We use bright field microscopy to observe the phase behavior of the base layer in a gravitationally confined colloidal system of silica particles. After injecting the colloidal particles into a chamber and giving the system sufficient amount of time for sedimentation, we observe those particles settling on the base of the chamber forming a static quasi-2D structure. We control two parameters of the system, namely the particle concentration and their Péclet number. The Péclet number measures the relative importance of the gravitational force over the thermal effects, and is positively related to the particle diameters. We find that the most ordered states are formed by the heavy particles (with large Péclet numbers) at moderately high concentrations. For the lighter particles with smaller Péclet numbers, we observe the 'glassy' phases in some sedimented quasi-2D colloidal systems, which do not exist in the ideal 2D hard disk fluids.

Crystals and Liquids in Gravitationally Confined Quasi-2-Dimensional Colloidal Systems

by

Yijun Dong

Eric Weeks

Advisor

A thesis submitted to the Faculty of Emory College of Arts and Sciences
of Emory University in partial fulfillment
of the requirements of the degree of
Bachelor of Sciences with Honors

Department of Physics

2018

Acknowledgements

I would like to thank my thesis advisor Dr. Eric Weeks for the enlightening guidance and patient support along the way.

I would like to thank my committee members. Thank you to my research advisor at Oxford College Dr. Effrosyni Seitaridou for the encouragement and help since my freshman year. Thank you to my collaborators Dr. James Kindt (and Peiyao Wu) for all the great suggestions and ideas.

I would like to thank Skanda Vivek and Carlos Orellana for teaching me all the useful experimental and computational techniques.

I would like to thank all the lab members and staff for their support and help in the past two years.

Table of Contents

List of Figures

Figure 9a The empty / sparse overlayer (EO) of a monodispersed sedimented system.

Figure 9b The single dilute overlayer (SDO) of a monodispersed sedimented system.

Figure 9c The multiple dilute overlayers (MDO) of a monodispersed sedimented system.

Figure 9d The multiple compact overlayers (MCO) of a monodispersed sedimented system.

Figure 9e The side views of the 4 categories of overlayers.

Figure 10a The mean square displacement curves and the corresponding overlayer densities of particles with $Pe = 24$ ($d = 1.85\ \mu m$).

Figure 10b The median ψ_6 and the corresponding overlayer densities of particles with $Pe = 24$ ($d = 1.85\ \mu m$).

Figure 10c The L_{ψ_6} and the corresponding overlayer densities of particles with $Pe = 24$ ($d = 1.85\ \mu m$).

Figure 11a The mean square displacement curves and the corresponding overlayer densities of particles with $Pe = 14$ ($d = 1.61\ \mu m$).

Figure 11b The median ψ_6 and the corresponding overlayer densities of particles with $Pe = 14$ ($d = 1.61\ \mu m$).

Figure 11c The L_{ψ_6} and the corresponding overlayer densities of particles with $Pe = 14$ ($d = 1.61\ \mu m$).

Figure 12a The mean square displacement curves and the corresponding overlayer densities of particles with $Pe = 13$ ($d = 1.58\ \mu m$).

Figure 12b The median ψ_6 and the corresponding overlayer densities of particles with $Pe = 13$ ($d = 1.58\ \mu m$).

Figure 12c The L_{ψ_6} and the corresponding overlayer densities of particles with $Pe = 13$ ($d = 1.58\ \mu m$).

1 Introduction

The transitions between the gas, liquid, and solid phases of matter are ubiquitous in nature [1]. From the freezing of water that forms ice to the crystallization of salt from seawater, the transitions between the liquid and solid phases of matter involve the change of particle ordering within the system. Meanwhile, colloids are suspensions of microscopically dispersed insoluble particles throughout a liquid [18]. The diameters of colloidal particles fall in a range between 1 nm and 10^3 nm [11], where the individual particles can be observed via the optical microscopy over accessible length and time scales. Colloid particles also display intriguing phase transitions between liquids and solids which have been an interesting research topic in the solid state physics for decades [1, 7]. A colloidal crystal is a highly ordered array of colloidal particles, analogous to the crystal lattice, that is able to extend for a large length scale [15]. Depending on the initial state and the dynamics of the phase transition, as the concentration increases, a 3D colloidal suspension may undergo crystallization and form ordered colloidal crystals, or be trapped in the amorphous gel-like state and form colloidal glasses [1, 18]. Since the advances in imaging techniques enable the direct observation of individual colloidal particles during the phase transition [1], the colloidal suspensions are commonly used as model systems in studying glass transition and crystallization of materials [18].

Growth of 3D colloidal crystals under sedimentation is an active research topic studied by various simulations and experiments [5, 10, 13, 14]. Meanwhile, research indicates that phase behaviors of 2D or quasi-2D systems can be modeled by colloidal suspensions confined in thin layers [15]. Particles with proper sizes and buoyant densities can be confined by the gravitational force in a monolayer, and thereby form a monolayer structure under sedimentation, as shown in Figure 1. The quasi-2D ordering of particles in such monolayer structures can be affected by the particle sizes, as well as the concentrations of sedimented systems. Specifically, gravitationally confined colloidal particles are dominated by two types of motions, namely the diffusion and sedimentation. The size of particles determines the relative importance between diffusion and sedimentation.

Qualitatively, for the 'heavy' large particles, sedimentation has more significant effects on the particles. Thus, the particles are prone to be confined by the gravity and form a monolayer structure. In contrast, for the 'light' small particles, diffusion dominates the motion of the particles. In this case, particles tend to fluctuate in the 3D space due to their thermal energy, and therefore are less probable to form quasi-2D structures.

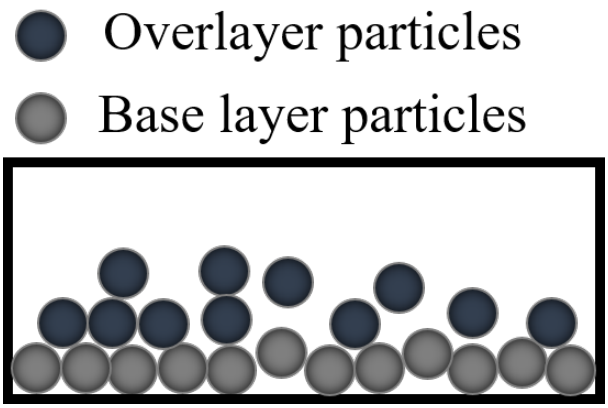

Figure 1: A sedimented colloidal system with a gravitationally confined monolayer structure over the base of the system.

An ideal 2D hard disk fluid has three different phases, the crystal phase, the liquid phase and an intermediate hexatic phase [3, 12]. Between these phases, the ideal 2D hard disks undergo two stages of phase transitions, the first-order liquid-hexatic transition and the second-order hexatic-solid transition [3]. Different from a 3D hard sphere system which can be trapped in a disordered glassy state, a 2D hard disk fluid does not have glassy phases. This is because the equilateral triangular local optimal packing of hard disks can tile the 2D space, while the tetrahedral local optimal packing of hard spheres fails to fill the 3D space [12]. Nevertheless, a real gravitationally confined quasi-2D monolayer structure may display different ordering behaviors from those of an ideal 2D system because of the particle diffusion in the vertical direction, the inevitable polydispersity of synthetic colloidal particles [2], and the effects of overlayer particles on the base layer ordering (Figure 1).

In this thesis we present a series of experiments where we use bright field microscopy to observe the phase behaviors of the base layer in a gravitationally confined colloidal system of monodispersed silica particles. After injecting the colloidal particles into a chamber

and giving the system sufficient amount of time for sedimentation, we observe those particles settling on the base of the chamber forming a stable or metastable monolayer structure. We control two parameters of the system, namely the concentration of particles and their Péclet number. The Péclet number measures the relative importance of the gravitational force over the thermal fluctuation, and is positively related to the particle diameter. We find that the most ordered states are formed by the heavy particles (with large Péclet numbers) at moderately high concentrations. In addition, for the lighter particles with smaller Péclet numbers, we observe the 'glassy' phases in some sedimented quasi-2D colloidal systems, which do not exist in the ideal 2D hard disk fluids.

2 Relevent Physics

2.1 Diffusion, Sedimentation, and the Péclet Number

The motion of heavy colloidal particles consists of the diffusion driven by the thermal energy and the sedimentation due to the gravitational potential. In a dilute suspension where the particle interaction is negligible, when the thermal fluctuation of the particles and the gravitational force reach an equilibrium, the distribution of particles with respect to the height can be expressed as,

$$P(z) = \frac{1}{l_g} \exp\Big(- \frac{z}{l_g}\Big), \tag{1}$$

where z denotes the height that particles reach from the base of a chamber. l_g (m) is the characteristic lengthscale that is related to the thermal energy and the gravitational force of the particle,

$$l_g = \frac{k_B T}{mg}, \tag{2}$$

where $k_B = 1.38 \times 10^{-23}\ J/K$ is the Boltzmann's constant; T represents the absolute temperature of the system in Kelvin; m (kg) denotes the buoyant mass of the particle; and $g = 9.8\ m/s^2$ is the gravitational acceleration.

From Equation (1), we can predict the probability of particles in a dilute system forming quasi-2D structures under sedimentation by comparing l_g with the particle diameter d. Roughly, we define the monolayer structure formed by particles that directly settle on the base as the base layer; and we name the other particles in the system that settle on or fluctuate above the base layer as the overlayer particles. For $d \leq l_g$, the probability for the particles to fluctuate above one particle diameter is large enough such that the particles are not expected to form a quasi-2D monolayer without the pressure from dense overlayers. However, when $d > l_g$, the probability of finding particles above one particle diameter due to thermal fluctuation is negligible. Therefore, the particles driven by the sedimentation are expected to form a monolayer structure in the base layer without

significant amounts of overlayer particles.

The Péclet number (Pe) is a dimensionless number that measures the relative importance of the gravitational potential over the thermal fluctuation on the particle motion,

$$Pe = \frac{d}{l_g} = \frac{\pi \Delta \rho g}{6 k_B T} \cdot d^4 \propto d^4, \tag{3}$$

where $\Delta\rho = \rho_{particle} - \rho_{media}$ is the buoyant density of the particles in the media. Equation (3) indicates that for a colloidal system with given uniform media at a certain temperature, the Péclet number of particles is positively related to the particle diameter, $Pe \propto d^4$. Together with Equation (1), we predict that in a monodispersed system of large particles with an appropriate concentration, an ordered quasi-2D structure will form in the base layer without the accumulation of particles in the overlayers under sedimentation because of the relatively large Péclet numbers (Equation (3)). However, a system of smaller particles will not form an ordered base layer unless the particle concentration in the overlayer is high enough to apply sufficient pressure on the base layer and constrain the diffusion of the base layer particles in the vertical direction.

2.2 Quasi-2D Ordering of Heavy Colloidal Particles

When $Pe(d) \gg 1$, the diffusion of particles in the vertical direction is negligible compared to the sedimentation. Given a proper concentration, all the particles will be confined to the base layer by the gravitational force, and the system can be mapped into two-dimension. Moreover, for the hard spherical particles, like the silica particles, the particle interaction is negligible unless the particles contact with each other, where they are strongly repulsive [18]. Therefore in the ideal case, a perfectly monodispersed system of large hard spherical particles ($Pe(d) \gg 1$) with a proper concentration can be well-represented by the hard disk fluid. The two-dimensional hard disk fluid has three different phases, the crystal phase with both long-range positional and orientational orders, the liquid phase where both positional and orientational correlations show exponential decays, and the intermediate hexatic phase with a power decay in the positional correlation [3, 12].

Simulations on the hard disk model indicate that the phase transition of the hard disk fluid consists of two stages, the first-order liquid-hexatic transition and the second-order hexatic-solid transition [3]. Moreover, different from the 3D hard sphere system which can be trapped in a disordered glassy state, the hard disk fluid does not have a glassy phase in two-dimension. This is because the equilateral triangular local optimal packing of hard disks can tile the 2D space, while the tetrahedral local optimal packing of hard spheres fails to fill the 3D space [12].

However, the 3D colloidal system confined by gravity has several complications compared with the ideal 2D hard disk model which may lead to different order behaviors. First, particles in the gravitationally confined colloidal system experience thermal fluctuation in the vertical direction, while the hard disk model assumes zero potential energy and thermal fluctuation in two-dimension only [3]. We predict that this variation has little effect on the colloidal systems of large particles because the diffusion is negligible compared with the sedimentation for large Péclet numbers (Equation (1), (3)). However, the variation becomes nontrivial for the systems of smaller colloidal particles where the thermal fluctuation dominates the particle motion. In this case, the real 3D colloidal system may have a distinct order behavior from the 2D hard disk fluid. The second complication comes from the polydispersity (i.e., the non-uniformity of particle sizes) of a real colloidal system. The diameters of real synthetic colloidal particles have a distribution that usually spreads more than $2-3\%$ of the average diameter [2]. The polydispersity has non-negligible effects on the crystallization of a colloidal system [2]. For instance, experiments on hard spherical colloidal particles suggest that the crystallization is impeded when the polydispersity exceeds 12% [16]. Due to these complications and their non-trivial effects on the order behaviors, we predict that a real sedimented quasi-2D colloidal system will have different phase behaviors depending on various factors, including the particle sizes and the polydispersity of the system.

In addition to the vertical thermal fluctuation and the polydispersity, different from the ideal 2D hard disk model, in a real sedimented 3D colloidal system, particles in the overlayer have critical effects on the crystalline packing in the base layer. The overlayer

particles can apply pressure on the base layer that promotes the crystalline packing. Specifically, the particles in the overlayer, provided a sufficient density, can inhibit the vertical fluctuation of the base layer particles by constraining their diffusion within the base layer. Nevertheless, particles in the overlayer may hinder the ordering of the base layer by impeding the particle motion and rearrangement in the base layer. Starting with a random disordered state, the base layer may be locked in a disordered phase by the concentrated overlayer, and form a 'glassy' state that does not exist in the 2D hard disk fluid.

3 Experimental Methods

We study the quasi-2D crystalline packing of gravitationally confined spherical particles by observing the base layer ordering of a sedimented monodispersed micrometer-scale silica particle suspension in water. The experiments consist of three parts, namely the preparation of a sedimented colloidal system, the microscopy for recording the base layer ordering, the image analysis and the particle tracking for analyzing the ordering behaviors.

3.1 Preparation of A Sedimented Colloidal System

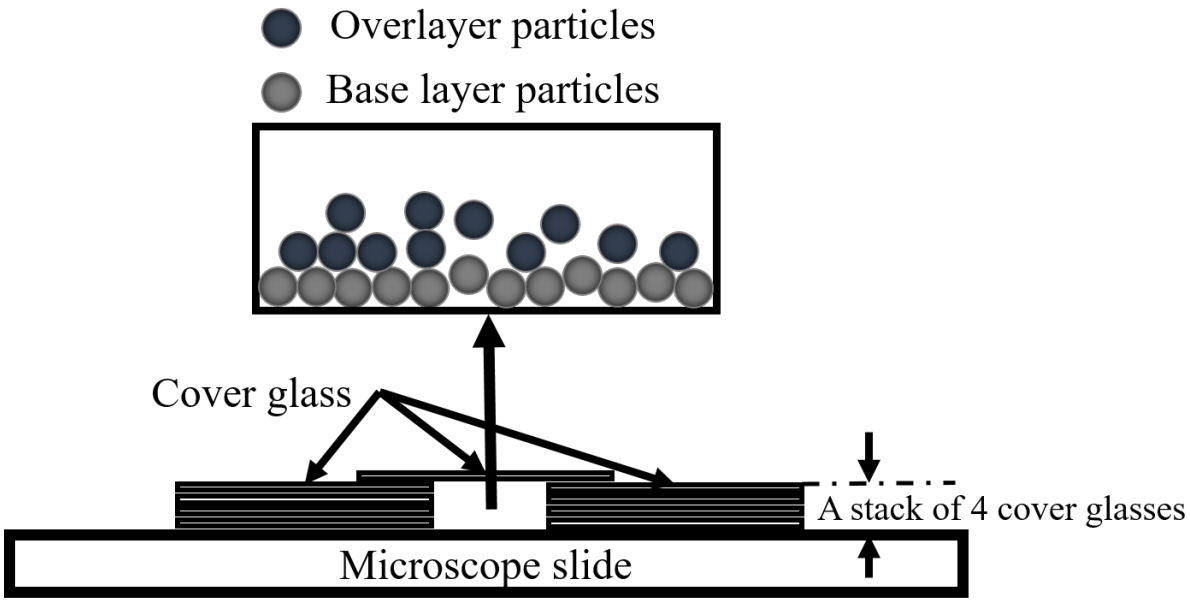

Figure 2: A sedimented monodispersed colloidal system in a chamber formed by a microscope slide and $(2 * n + 1) = 9$ $(n = 4)$ pieces of cover glasses that are adhered and sealed by the Norland optical adhesive.

We prepare a sedimented colloidal system starting with a 3D colloidal system, by giving the system sufficient amount of time to reach a stable or quasi-stable state under sedimentation. First, we inject a suspension of colloidal particles in water into a chamber formed by a microscope slide and cover glasses, and then adhere and seal the chamber using the Norland optical adhesive, as shown in Figure 2. Then the 3D colloidal suspension is well mixed by hand shaking, as well as by flipping the chamber up-side-down. We

let the well-mixed 3D colloidal system rest on a horizontal surface (usually a horizontal microscope stage) for sufficiently long time (usually $15 - 30$ minutes), and allow the system to form a stable or quasi-stable state under sedimentation.

We roughly control the area fraction of the base layer in a sedimented colloidal system by adjusting the height of the chamber and the concentration of the colloidal suspension injected into the chamber. The height of the chamber is adjusted discretely by stacking various numbers of cover glasses (e.g., 4 cover glasses in Figure 2) at the side boundaries of the chamber. Specifically, for a monodispersed colloidal suspension with particle concentration n (mm^{-3}) confined in a chamber with height h (mm) as shown in Figure 2, a_0 (mm^2) denotes the area of the projection of a spherical particle on the horizontal surface. When n is in a moderate range such that all the particles in the 3D suspension are able to settle in the base layer without occupying the space in the overlayer, then the upper bound, ϕ_{max}, of the base layer area fraction, ϕ, are given by,

$$\phi \leq \phi_{max} = \frac{nVa_0}{A} = a_0 nh, \tag{4}$$

where V (mm^3) and A (mm^2) are the total volume of the 3D suspension and the base layer area of the chamber, respectively, such that $h = V/A$. Meanwhile, for a given h, when n is large enough such that the particles stack in the overlayer after fully spanning the base layer, we are able to adjust the overlayer particle concentration by changing the concentration n. The base layer area fraction of such a concentrated sedimented system varies from moderate to high depending on the ordering of the base layer.

Table 1: The diameters of spherical silica particles and their corresponding Peclet numbers. We assume that the silica particles are suspending in water at the room temperature.

d (μm)	1.85	1.61	1.58
Pe	24	14	13

Furthermore, to investigate the effect of the Peclet number on the base layer ordering, we prepare monodispersed colloidal systems with spherical sillica particles of various diameters, as shown in Table 1. The particles with diameter $d = 1.85$ μm and 1.61 μm are non-functionalized silica microspheres with natural hydroxyl or silanol surface groups

manufactured by the Bangs Laboratories Inc. These particles typically have coefficients of variance (C.V.) of $10-15\%$ in their diameters. The silica microspheres with diameter $d = 1.58\ \mu m$ are produced by the Duke Scientific Corporation. These particles are composed of amorphous silica with no surface additives. The particle diameter has a standard deviation of $0.04\ \mu m$, corresponding to a C.V. of 2.5%.

3.2 Microscopy

We observe the ordering of the base layer in a sedimented colloidal system in the stable or quasi-stable state using bright field microscopy with a $100\times$ oil lens and Köhler illumination. Specifically, we record the constrained diffusion process of particles in the base layer using a high-speed camera connected to the microscope, for $1-5$ minutes with a frame frequency of $4s^{-1}$, corresponding to an inter-frame time interval of $\Delta t = 0.25\ s$. The regions in the base layer observed by the microscope are square frames with side lengths within the range $70-130\ \mu m$, or $40-90$ particle diameters, which contains around $1000-4000$ particles. The Köhler illumination is a sample illumination technique that provides even illumination with high sample contrast [9]. By applying the Köhler illumination, we are able to distinguish the base layer particles from the background, as well as the overlayer particles, and thereby observe the particle ordering and motion in the monolayer structure.

3.3 Particle Identification, Tracking, and Phase Analysis

Via a series of image processing and particle tracking algorithms in IDL (i.e., Interactive Data Language) developed by Crocker and Grier [4], we are able to extract quantitative data on the structures and dynamics of colloidal suspensions in various phases from the digital video microscope images [8]. First, the particles are identified, located, and refined iteratively based on the brightness-weighted centroid estimation [4]. This method is limited by the digital image resolution and the noise in the original image (e.g., the shadows of inter-layer particles fluctuating between the base layer and the overlayer), but is not sensitive to the optical resolution of the microscope (e.g., 200 nm for a typical

100× objective) [8]. Specifically, the algorithms can determine the particle positions up to a remarkable precision of $30-50$ nm [8], which is negligible compared to the diameters of the colloidal particles. Furthermore, the algorithms support simultaneous tracking of several thousands of particles from the particle position data [8]. The trajectory linking from the particle positions is based on considering the dynamics of the noninteracting Brownian particles [4].

From the particle position data, we are able to further analyze different phase properties of the monolayer structures in the sedimented colloidal systems, including the base layer area fraction and the measurement of 2D hexagonal packing, ψ_6. The monolayer area fraction ϕ is evaluated from the particle diameter d in and the particle count N in a given frame with known total area A,

$$\phi = \frac{\pi d^2 N}{4A}. \tag{5}$$

Meanwhile, the measurement of 2D hexagonal packing, ψ_6, is calculated in two steps. First, the monolayer is partitioned with respect to the set of particle positions using the Delaunay triangulation. A pair of particles connected by an edge of a triangle in the partition is defined as neighbors. Knowing the position of a given particle and all its neighbors, we can conduct further phase analysis on the ordering of particles in the monolayer which will be introduced in Section 4.1.

4 Analysis Methods

4.1 Two-Dimensional Crystalline Packing

We use ψ_6 as an order parameter to quantify ordering of a two-dimensional structure. The ψ_6 is a normalized complex number that measures the hexagonal packing of the two-dimensional monodispersed particles,

$$\psi_6 = \frac{1}{N} \sum_{k=1}^{N} \exp(i \cdot 6\theta_k), \tag{6}$$

where given a fixed axis and a 2D projection of a particle, k spans all the immediate neighbors of the given particle determined by the Delaunay triangulation; N denotes the total number of neighbors of the particle; and θ_k represents the angle formed by the given axis and the connection of centers between the particle and its k-th neighbor, as shown in Figure 3a. Specifically, for our microscopic images (Section 3.2), we identify the position of a given particle and all its neighbors via the methods described in Section 3.3, and then calculate ψ_6 by taking the vertical and horizontal edges of the rectangular image frame as the fixed axis.

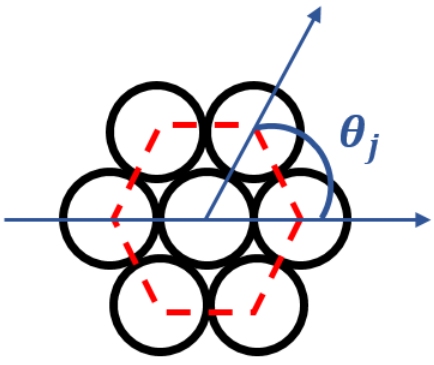

(a) A unit of two-dimensional crystal formed by 7 monodispersed particles in perfect hexagonal crystalline packing. The central particle has $|\psi_6| = 1$ with a phase angle of 0°.

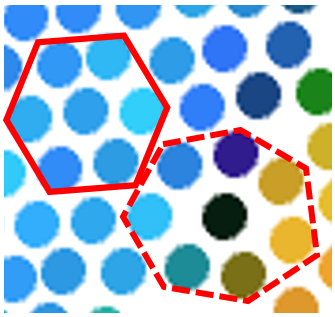

(b) The ψ_6 colorplot of a domain with both the 2D crystal in hexagonal packing, as labeled by the solid red boundary, and the grain boundary in disordered arrangement, as marked by the dash line. The ψ_6 color plot uses colors with high brightness to mark the particles with $|\psi_6| \to 1$. The particles with similar ψ_6 phase angles are labeled in similar colors (i.e., colors with similar hue values).

Figure 3: (3a) The definition of ψ_6, and (3b) a demonstration of the ψ_6 colorplot of a domain with both the 2D crystalline packing and the grain boundary.

In an ordered domain with the hexagonal 2D crystalline packing, particles have ψ_6 with absolute values $|\psi_6| \to 1$ and similar phase angles with respect to the common given axis (Figure 3a). In order to visualize the ordered and disordered domains within a 2D frame, we label particles with different $|\psi_6|$ and phase angles using different brightness and hue, respectively, as shown in Figure 3b.

Moreover, we define a correlation function on ψ_6 to approximate the average size of the ordered domains, as labeled by the solid red line segments in Figure 4a and 4c, within a frame. The ψ_6 correlation function $f : \mathbb{R}^+ \to [-1, 1]$ is defined such that,

$$f(r) = \langle \vec{\psi_6}(r) \cdot \vec{\psi_6}(0) \rangle, \tag{7}$$

where for a given particle with $\vec{\psi_6}(0) = a_0 + ib_0$ and any particle with $\vec{\psi_6}(r) = a_r + ib_r$ and distance r apart from the given particle,

$$\vec{\psi_6}(r) \cdot \vec{\psi_6}(0) = a_0 a_r + b_0 b_r. \tag{8}$$

The brackets $\langle \cdot \rangle$ denotes the average over all the possible pairs with distance r contained in the frame. The ψ_6 correlation function f usually shows an exponential decay as the distance r increases, as Figure 4b and 4d demonstrated. The average size of the ordered domains in a given frame is approximated by the fitting parameter in the exponent, named the ψ_6 characteristic length scale L_{ψ_6}, when the ψ_6 correlation data are fitted to an exponential decay,

$$f(r) = A \cdot \exp\Big(- \frac{r}{L_{\psi_6}} \Big), \tag{9}$$

as illustrated in Figure 4b and 4d.

4.2 Diffusion and Caging

Structural rearrangements and particle mobility are crucial properties of colloidal glasses and crystals that control the resistance to flow [17]. The mobility of particles in colloidal glasses is many orders of magnitude lower than those in fluids [17]. Therefore,

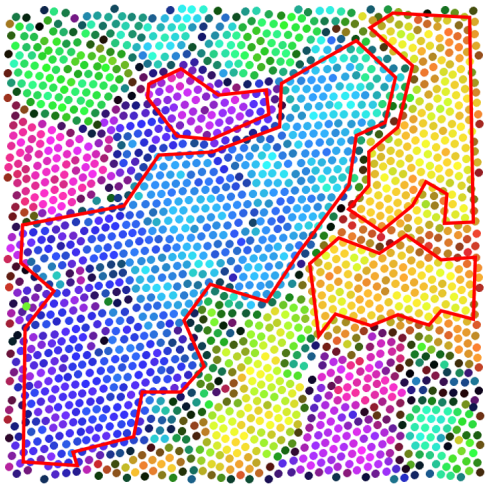

(a) The ψ_6 colorplot of a relatively ordered monolayer of particles with diameter $d = 1.58\ \mu m$ that contains large crystallized domains of various sizes, as marked by the solid red boundaries.

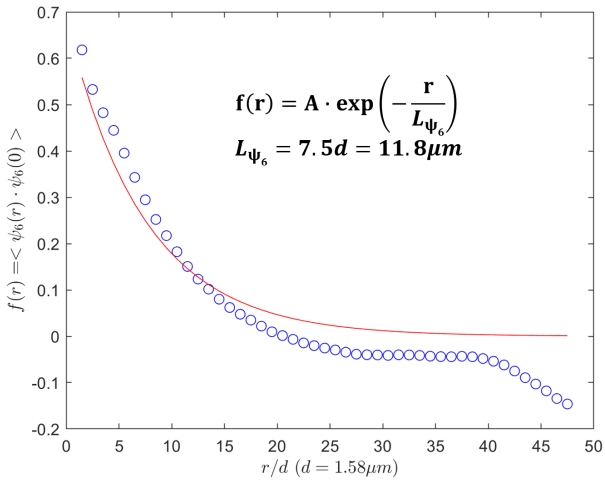

(b) The ψ_6 correlation function of particles in Figure 4a and the corresponding exponential decay predicted by Equation (9). From the fitting parameter, the approximated average size of the ordered domains, $L_{\psi_6} = 11.8\ \mu m = 6.4\ d$.

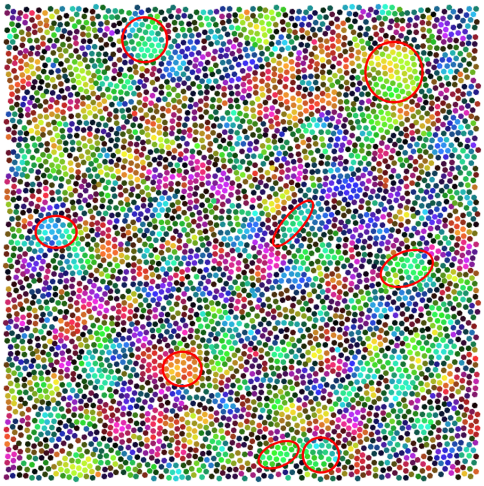

(c) The ψ_6 colorplot of a disordered monolayer of particles with diameter $d = 1.58\ \mu m$ that contains small crystallized domains of various sizes, as marked by the solid red boundaries.

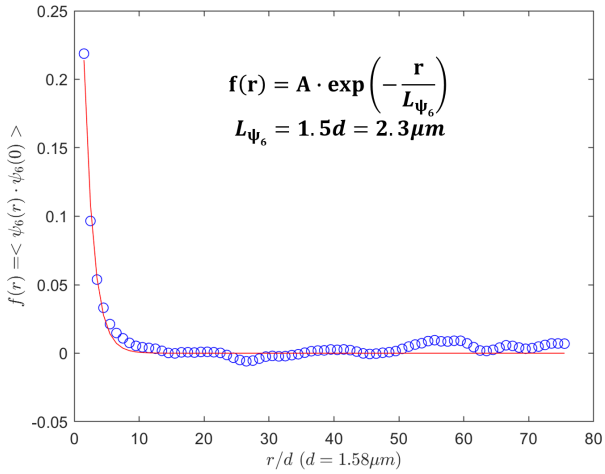

(d) The ψ_6 correlation function of particles in Figure 4c and the corresponding exponential decay predicted by Equation (9). From the fitting parameter, the approximated average size of the ordered domains, $L_{\psi_6} = 2.3\ \mu m = 1.5\ d$.

Figure 4: For a given relatively ordered (4a) or disordered (4c) frame, the average sizes of the ordered domains, L_{ψ_6}, are approximated from (4b, 4d) the corresponding ψ_6 correlation functions and their patterns of exponential decay given by Equation (9).

the particle mobility in the base layer of a sedimented colloidal system can be a potential indicator for the ordering of a gravitationally confined quasi-2D structure. We quantify the base layer particle mobility via the mean square displacement of particles undergoing

constrained diffusion,

$$\langle \Delta r^2 \rangle (\Delta t) = \langle [r(t + \Delta t) - r(t)]^2 \rangle_t, \tag{10}$$

where $\langle \cdot \rangle_t$ denotes the average of all the time intervals, starting from an arbitrary time t, with given length Δt.

For a 2D colloidal system in liquid phase, the free diffusion of particles is known as Brownian motion, which satisfies that [6],

$$\langle \Delta r^2 \rangle = \langle \Delta x^2 + \Delta y^2 \rangle \propto \Delta t. \tag{11}$$

However, in a concentrated system where the particle diffusion is significantly constrained by the neighbors, $\langle \Delta r^2 \rangle$ is not always proportional to Δt. In fact, the mean square displacements follow Equation (11) in a sufficiently small time interval before the particles start colliding with their neighbors, and also in a large enough time interval where the particles readily break the 'cages' formed by their neighbors via rearrangements. However, Equation (11) does not hold for the time intervals with intermediate lengths where particles are doing constrained diffusion in the 'cages' formed by the neighboring particles. Known as caging, for these intermediate-length time intervals,

$$\langle \Delta r^2 \rangle \propto \Delta t^k, \tag{12}$$

where $k \in (0, 1)$. In a $\log - \log$ plot of mean square displacements,

$$\log \langle \Delta r^2 \rangle = k \log \Delta t + c \tag{13}$$

for some constant c. From Equation (13), we can predict that a mean square displacement curve of the constrained diffusion will have slopes $k = 1$ at extremely short or long time intervals, while at the intermediate values of Δt, the curve has a plateau with $0 < k < 1$. For the base layer of a concentrated sedimented colloidal system, the slope and the height of the plateau in the mean square displacement curve reflect the mobility, as well as the average size of the 'cages', of the particles in the base layer.

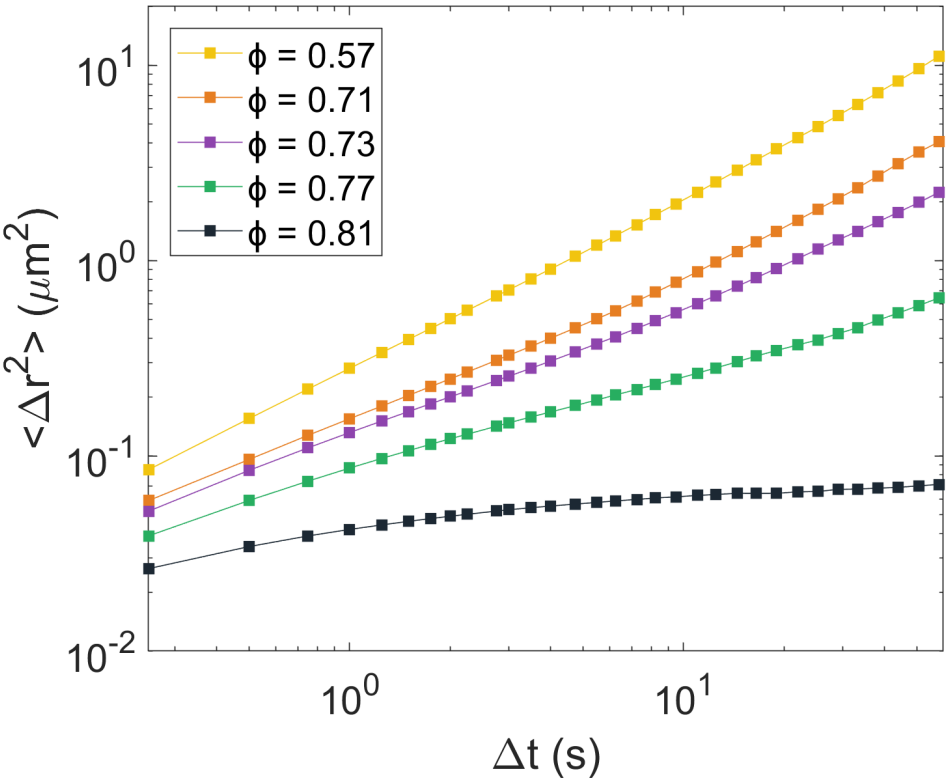

Figure 5: The mean square displacements (in a log − log plot) of the constrained particle diffusion in the base layers concentrated sedimented colloidal systems with different base layer area fractions. The set of curves shows the range of Δt while the particles are in the caging stage (i.e., $k < 1$ for Equation (12)). All the sediments systems are monodispersed with the particle diameter $d = 1.85\ \mu m$.

We use the particle tracking data (Section 3.3) extracted from the digital microscopic images (Section 3.2) to study the dynamics of the base layers in sedimented colloidal systems. Specifically, we first evaluate the mean square displacements of the particles via the `msd.pro` function implemented in the IDL particle tracking package [4]. Then we infer the particle mobility and rearrangements in different systems by comparing their corresponding mean square displacement curves (Figure 5).

Figure 5 illustrates a set of mean square displacement curves for the constrained diffusion of particles in the base layers with various area fractions. In Figure 5, both the slope and the height of the plateau decrease as the area fraction increases, because of the shrinking sizes of the 'cages' and the decrease in particle mobility when the system is approaching crystallization or glass transition.

5 Results

We investigate the base layer ordering of sedimented monodispersed colloidal systems with 3 different particle diameters (Table 1) and various base layer area fractions. We observe different base layer ordering behaviors as the area fraction increases for particles with small Péclet numbers (i.e., $Pe = 13, 14$) and those with relatively large Péclet numbers (i.e., $Pe = 24$). To understand the different ordering behaviors, we further analyze the particle density in the overlayer and the mobility in the base layer.

5.1 Base Layer Ordering Behaviors

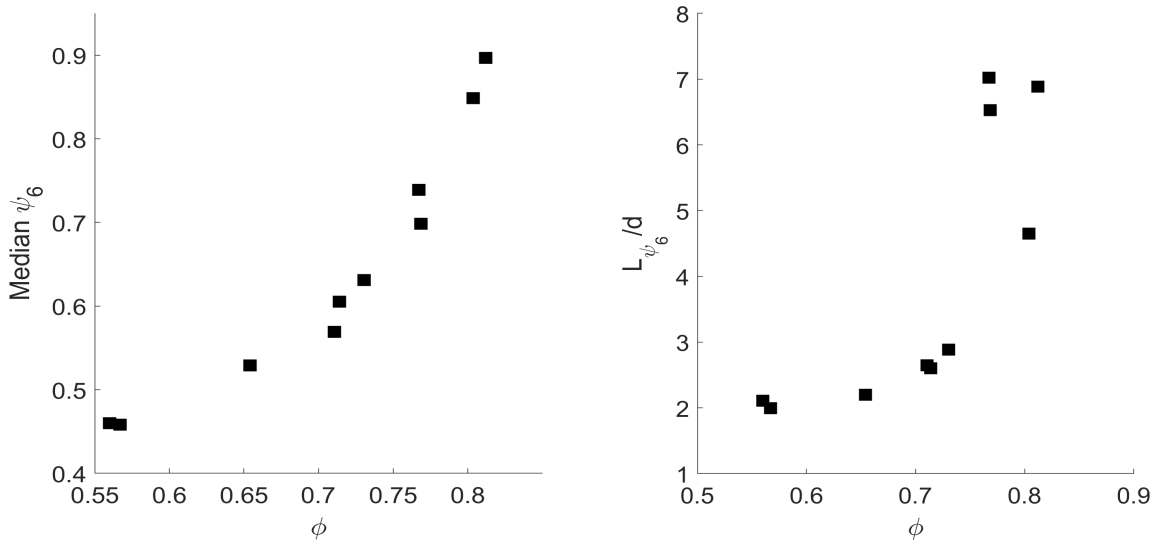

(a) The median ψ_6 of particles with $Pe = 24$ ($d = 1.85\mu m$).

(b) The L_{ψ_6} of particles with $Pe = 24$ ($d = 1.85\ \mu m$).

Figure 6: The base layer ordering of particles with $Pe = 24$ ($d = 1.85\ \mu m$). The base layer is more ordered as the area fraction increases. The most ordered phase is found at the highest area fraction. Each data point in the figures represents the average (i.e., area fraction, median ψ_6 and L_{ψ_6}) of $200 - 1000$ frames in a video as described in Section 3.2. The standard deviations of the area fraction, median ψ_6, and L_{ψ_6}/d for each data point are small, and therefore can approximately be represented by the size of the markers. The same is true for Figure 7 and Figure 8.

Figure 6, 7 and 8 demonstrate the median ψ_6 and normalized characteristic length scale L_{ψ_6}/d of the base layers in stable or metastable monodispersed sedimented colloidal suspensions with three different particle diameters, corresponding to a relatively large Péclet number $Pe = 24$ and two relatively small Péclet numbers $Pe = 14$ and 13.

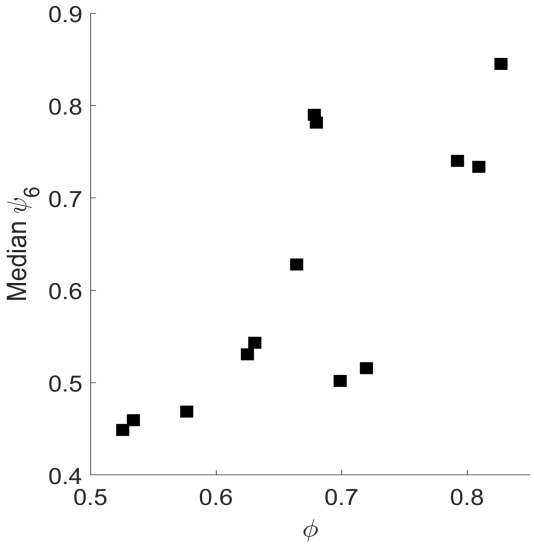

(a) The median ψ_6 of particles with $Pe = 14$ ($d = 1.61$ μm).

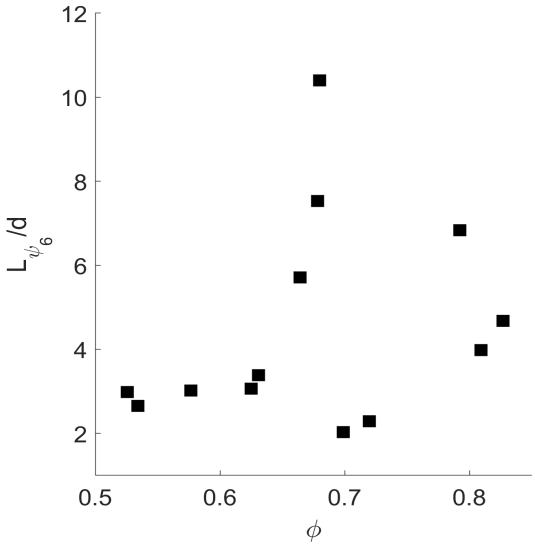

(b) The L_{ψ_6} of particles with $Pe = 14$ ($d = 1.61$ μm).

Figure 7: The base layer ordering of particles with $Pe = 14$ ($d = 1.61$ μm). Two sets of data are observed at the lower (i.e., $\phi \in (0.52, 0.69)$) and higher (i.e., $\phi \in (0.69, 0.83)$) area fraction intervals. The highly ordered phases can be found at both the highest and the intermediate area fractions. A wide range of ordering behaviors, from a highly ordered packing to a disordered phase, is observed in the interval of intermediate area fraction, $\phi \in (0.66, 0.72)$.

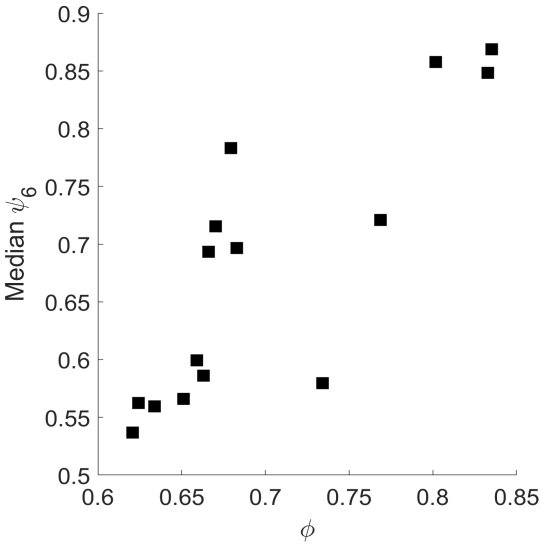

(a) The median ψ_6 of particles with $Pe = 13$ ($d = 1.58$ μm).

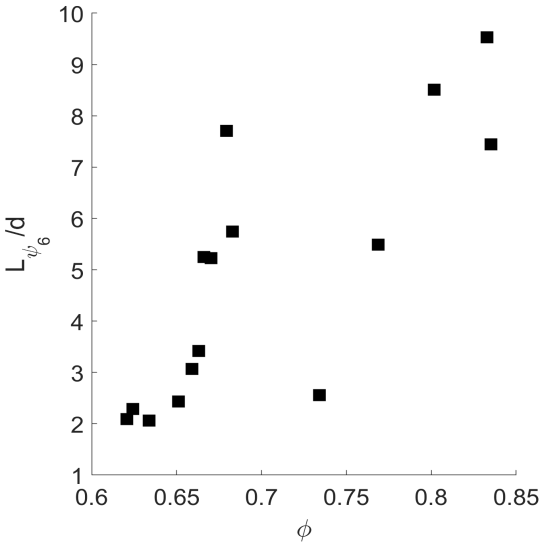

(b) The L_{ψ_6} of particles with $Pe = 13$ ($d = 1.58$ μm).

Figure 8: The base layer ordering of particles with $Pe = 13$ ($d = 1.58$ μm). Two sets of data are observed at the lower (i.e., $\phi \in (0.61, 0.70)$) and higher (i.e., $\phi \in (0.73, 0.84)$) area fraction intervals. The highly ordered phases can be found at both the highest and the intermediate area fractions. A wide range of ordering behaviors, from a highly ordered packing to a disordered phase, is observed in the interval of intermediate area fraction, $\phi \in (0.66, 0.74)$.

Specifically, as shown in Figure 6, for particles with diameter $d = 1.85\ \mu m$, corresponding to a relatively large Péclet number $Pe = 24$, the base layer of a sedimented system becomes more ordered with increasing area fraction. The most ordered packing is found in the sedimented system with the highest base layer area fraction. However, the base layer ordering of particles with smaller Péclet numbers, $Pe = 14$ ($d = 1.61\ \mu m$) and $Pe = 13$ ($d = 1.58\ \mu m$), does not show the same simple monotone pattern as the area fraction increase. As Figure 7 and Figure 8 indicate, for both of the relatively small Péclet numbers, two sets of data are observed at the lower and higher area fraction intervals. Highly ordered packings with median $\psi_6 > 0.7$ and $L_{\psi_6} > 6d$ can be found at both the highest and the intermediate area fractions. Moreover, wide ranges of ordering behaviors, from highly ordered packings to disordered phases, are observed in the intermediate area fraction intervals around $\phi \in (0.65, 0.75)$.

5.2 Overlayer Particle Density and Classification

In contrast to a 2D colloidal system, in a 3D sedimented colloidal suspension, particles in the overlayer may considerably affect the crystalline packing in the base layer. To understand the irregular ordering behaviors of the particles with relatively small Péclet numbers in sedimented colloidal systems with intermediate base layer area fractions (Figure 7 and Figure 8), we observe the overlayer by gradually adjusting the height of the focal plane starting from the base layer until a relatively well-defined overlayer is in focus and distinguishable from the base layer, as shown in Figure 9. Then we qualitatively estimate the particle density in the overlayer and classify the overlayers into four categories based on their density, numbered $1-4$ representing increasing particle density, as illustrated in Table 2. In general, we find denser overlayers in the more concentrated sedimented colloidal systems. The detailed effects of overlayers on the base layer ordering will be illustrated in Section 5.3.

Table 2: The four categories of overlayers, numbered $1-4$ with increasing particle density, classified qualitatively by scanning the overlayers and approximating the particle concentrations.

NO.	Classification	Description	Example
1	EO	Empty / sparse overlayer	Figure 9a
2	SDO	Single dilute overlayer	Figure 9b
3	MDO	Multiple dilute overlayers	Figure 9c
4	MCO	Multiple compact overlayers	Figure 9d

5.3 Base Layer Particle Mobility

Aiming to relate the overlayer particle density to different base layer ordering behaviors, we measure the base layer particle mobility via the mean square displacements (Equation (10)) and investigate the effect of the overlayer particles on the mobility in the base layer, as predicted in Section 4.2. Figure 10, 11 and 12 demonstrate the mean square displacement curves, along with the corresponding base layer ordering and the overlayer particle densities, for various base layer ordering behaviors of particles with different Péclet numbers, $Pe = 24, 14$ and 13. In the mean square displacements, the

median ψ_6 and the L_{ψ_6} plots, the markers of the same color represent the same base layer of a sedimented colloidal system. The sizes of the markers correspond to the particle densities in the overlayer, as labeled by the numbers (referring to Table 2) on the side of the markers in the median ψ_6 plots. For the relatively small Péclet numbers $Pe = 13$ and 14 where two sets of data at the lower and higher area fraction intervals are observed, we use the circular and the triangular markers to represents the data in the lower and higher area fractions, respectively.

For particles with $Pe = 24$, the base layer mobility decreases as the overlayer particle density increases, as shown in Figure 10a. Meanwhile, we find that the base layer tends to be more ordered for lower mobility by comparing Figure 10a with Figure 10b and 10c.

For particles with $Pe = 14$, the base layer mobility also shows a decrease as the overlayer particle density increases. The median ψ_6 tends to increase as the mobility decreases. However, L_{ψ_6} is prone to be smaller for the lower mobility and denser overlayer, as illustrated by the grey and black triangular data point in Figure 11.

For particles with $Pe = 13$, the base layer mobility decreases with increasing overlayer particle density in general. The only exception takes place between the violet circular and the black triangular data points in Figure 12, where the difference in the base layer area fraction plays a more important role in the mobility. In contrast to the particles with larger Péclet numbers ($Pe = 24$ and 14), for the particles with $Pe = 13$, the base layer ordering fails to show a monotone pattern with respect to the change in the particle mobility. Particularly, in Figure 12, the orange circular and the blue triangular data points are in the disordered phases with dense overlayers and especially low mobilities compared to other data points in the more ordered phases with higher area fractions (e.g., the violet circular, red circular, green triangular, and black triangular data points).

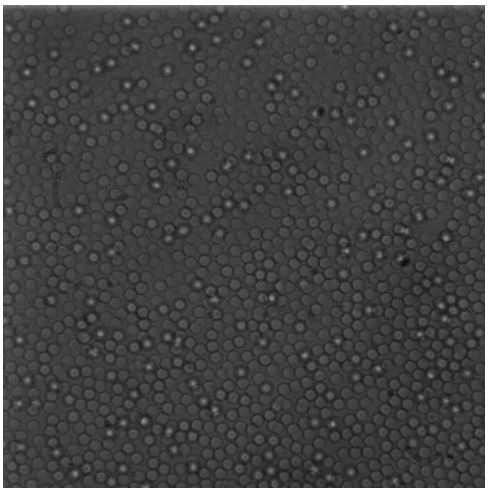

(a) The empty / sparse overlayer (EO) of a monodispersed sedimented system with particle diameter $d = 1.85\ \mu m$ with a 150× magnification.

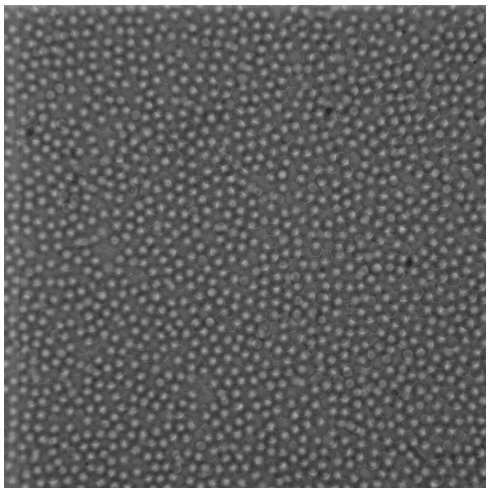

(b) The single dilute overlayer (SDO) of a monodispersed sedimented system with particle diameter $d = 1.85\ \mu m$ with a 150× magnification.

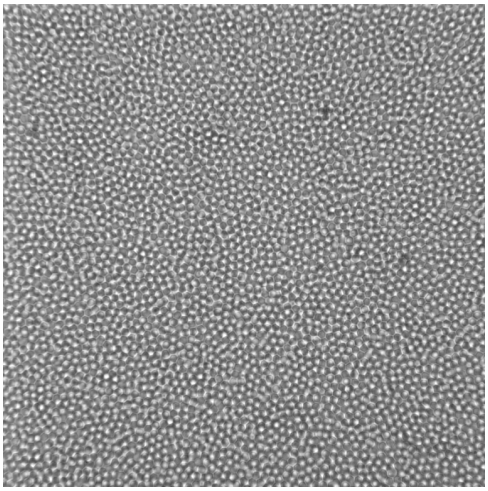

(c) The multiple dilute overlayers (MDO) of a monodispersed sedimented system with particle diameter $d = 1.85\ \mu m$ with a 100× magnification.

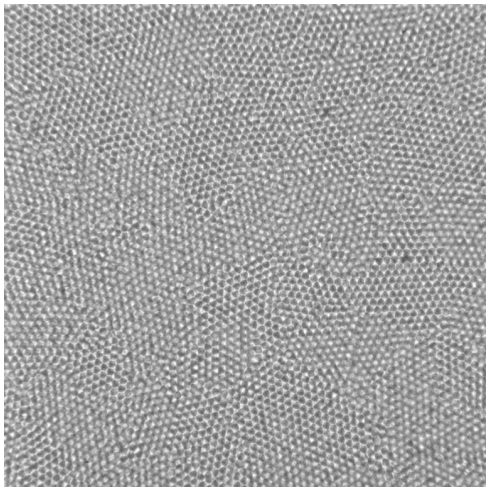

(d) The multiple compact overlayers (MCO) of a monodispersed sedimented system with particle diameter $d = 1.85\ \mu m$ with a 100× magnification.

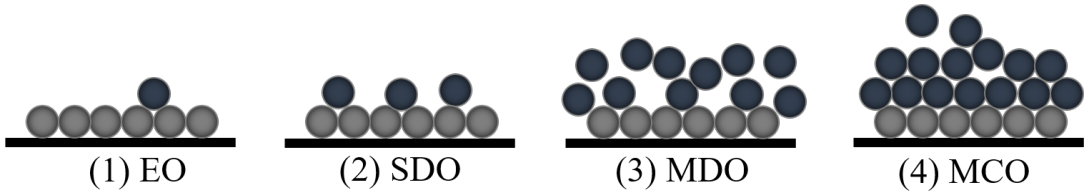

(e) The side views of the 4 categories of overlayers.

Figure 9: Four categories of overlayers classified by their particle densities. Figure 9a, 9b, 9c and 9d are the digital microscopic images of different categories of overlayers. The particles with relatively bright (white) centroids are the overlayer particles that are in focus. The base layer particles, as well as some overlayer particles, that are out of focus appear as the dim contours and transparent interiors with the similar color as that of the background. Figure 9e demonstrates the approximated side-views of the four types of overlayers.

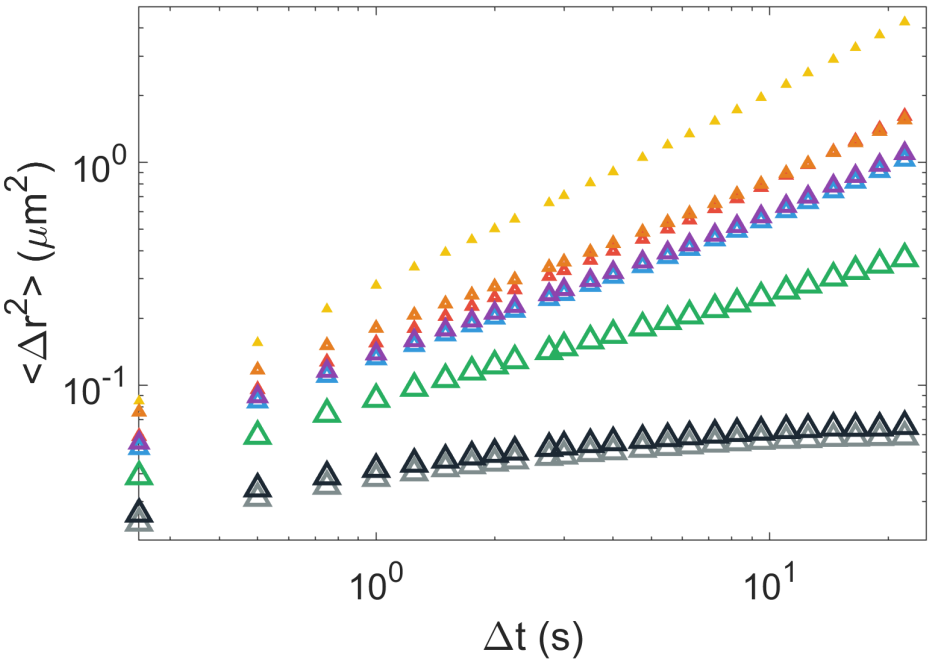

(a) The mean square displacement curves and the corresponding overlayer densities of particles with $Pe = 24$ ($d = 1.85\ \mu m$).

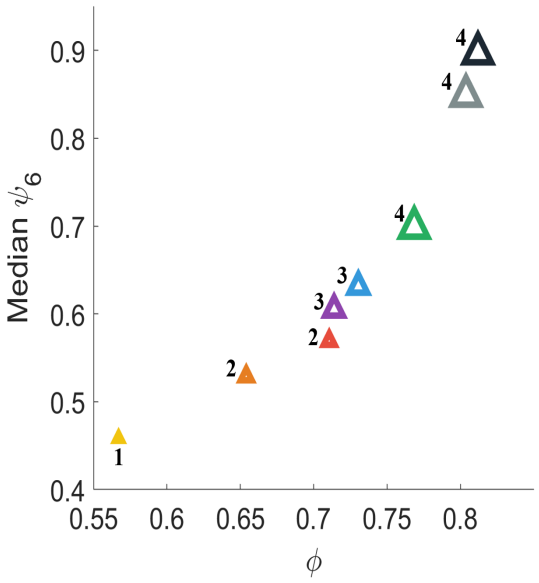

(b) The median ψ_6 and the corresponding overlayer densities of particles with $Pe = 24$ ($d = 1.85\ \mu m$).

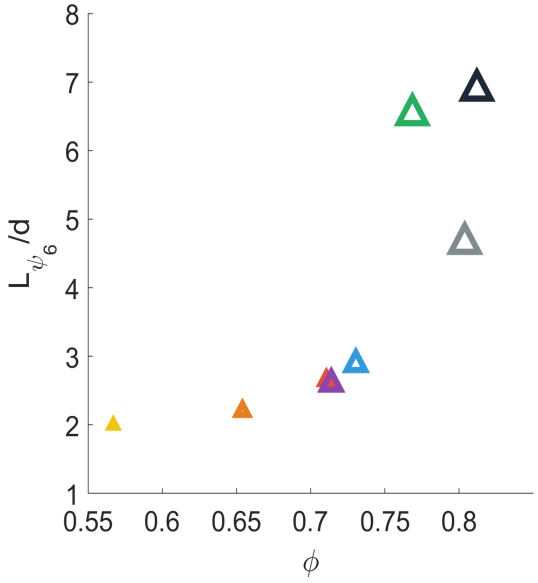

(c) The L_{ψ_6} and the corresponding overlayer densities of particles with $Pe = 24$ ($d = 1.85\ \mu m$).

Figure 10: The mean square displacement curves, the base layer ordering and the corresponding overlayer densities of particles with $Pe = 24$ ($d = 1.85\ \mu m$). As the overlayer particle density increases, the mobility in the base layer decreases and the base layer tends to be more ordered.

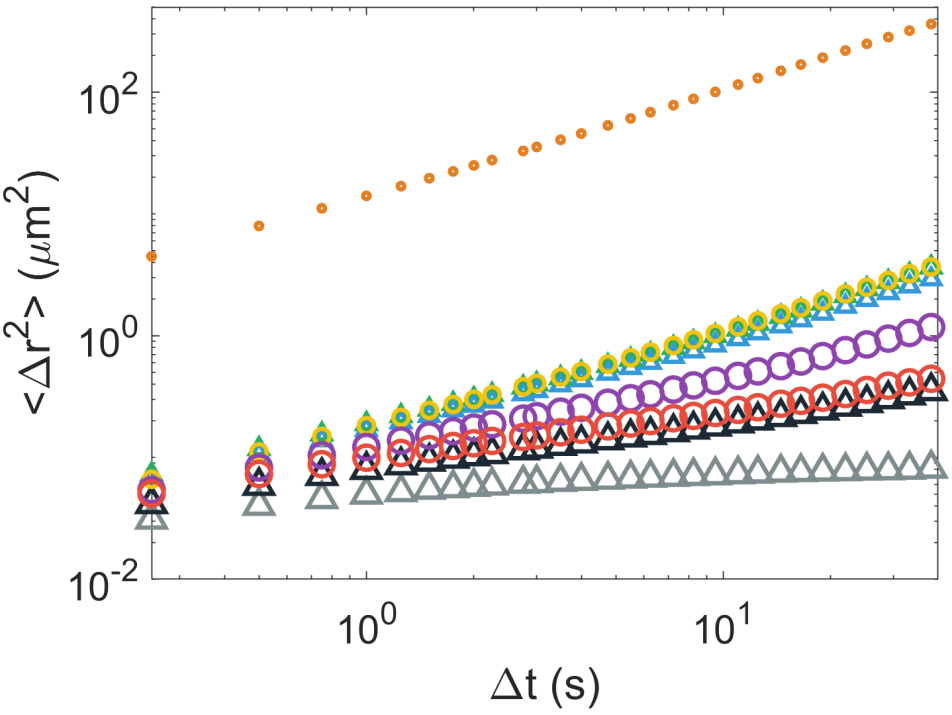

(a) The mean square displacement curves and the corresponding overlayer densities of particles with $Pe = 14$ ($d = 1.61$ μm).

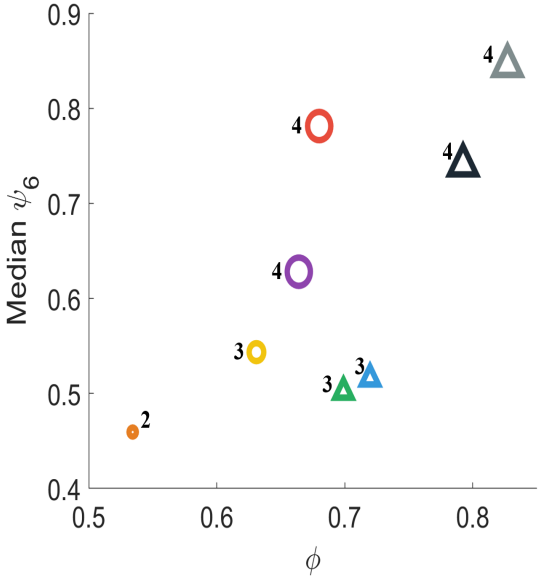

(b) The median ψ_6 and the corresponding overlayer densities of particles with $Pe = 14$ ($d = 1.61$ μm).

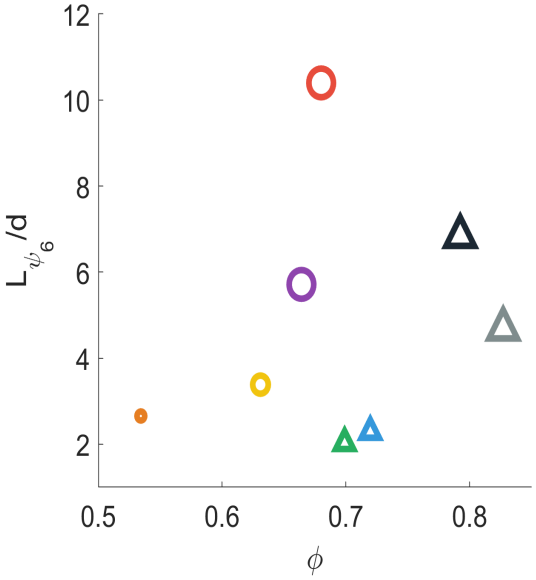

(c) The L_{ψ_6} and the corresponding overlayer densities of particles with $Pe = 14$ ($d = 1.61$ μm).

Figure 11: The mean square displacement curves, the base layer ordering and the corresponding overlayer densities of particles with $Pe = 14$ ($d = 1.61$ μm). As the overlayer particle density increases, the mobility in the base layer decreases. In terms of the base layer ordering, the median ψ_6 tends to increase as the mobility decreases. However, L_{ψ_6} tends to be smaller for the lower mobility and denser overlayer, as illustrated by the grey and black triangular data point.

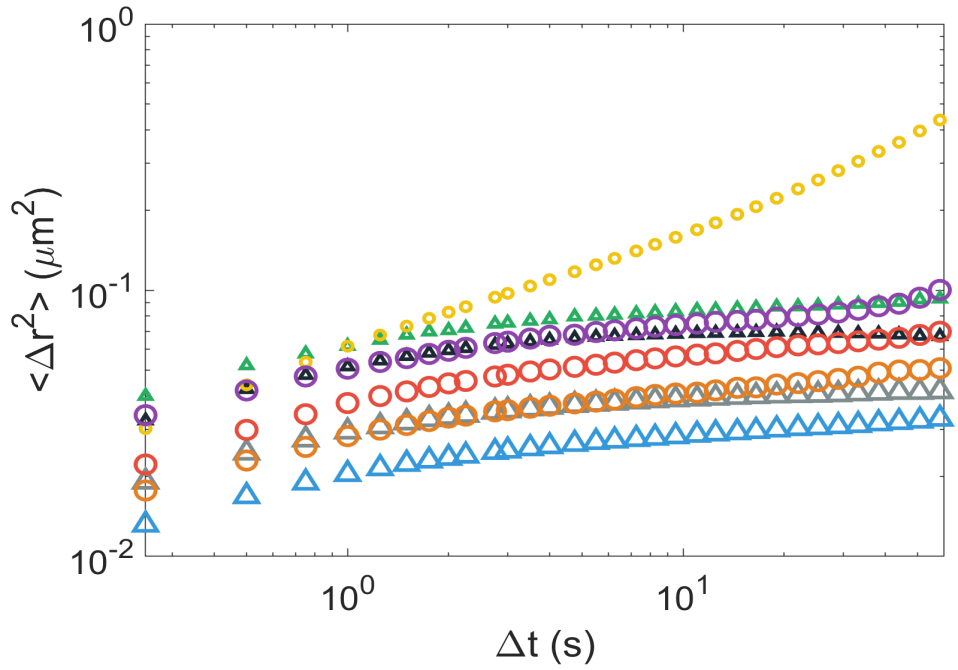

(a) The mean square displacement curves and the corresponding overlayer densities of particles with $Pe = 13$ ($d = 1.58$ μm).

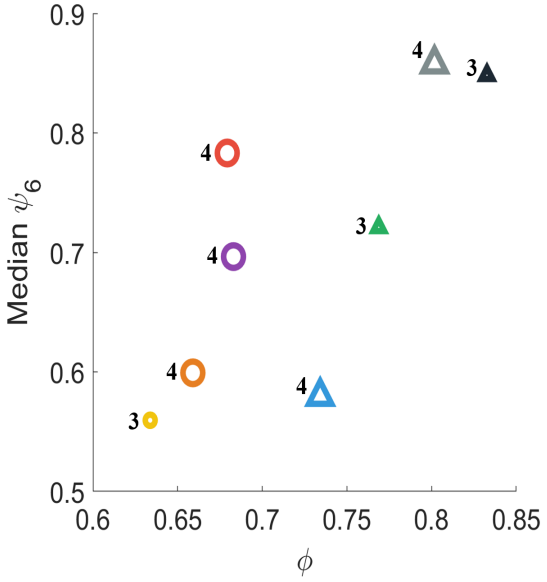

(b) The median ψ_6 and the corresponding overlayer densities of particles with $Pe = 13$ ($d = 1.58$ μm).

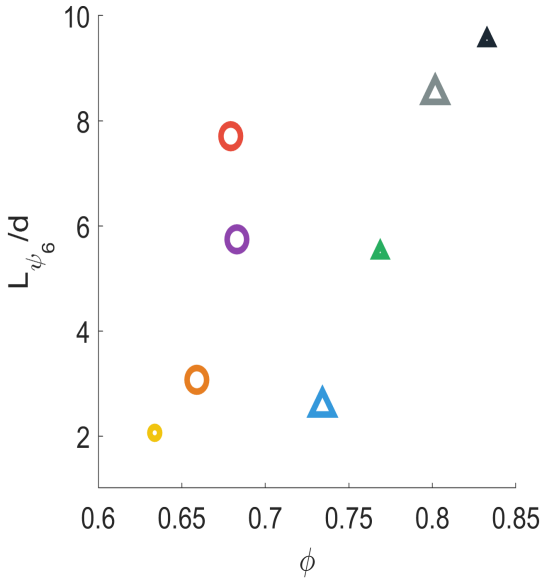

(c) The L_{ψ_6} and the corresponding overlayer densities of particles with $Pe = 13$ ($d = 1.58$ μm).

Figure 12: The mean square displacement curves, the base layer ordering and the corresponding overlayer densities of particles with $Pe = 13$ ($d = 1.58$ μm). The base layer particle mobility decreases as the density of the overlayer increases. The only exception take place between the violet circular data point and the black triangular data point, where the difference in the base layer area fraction has considerable effects on the mobility. The base layer ordering does not show a monotone pattern as the mobility decreases. Particularly, the orange circular and the blue triangular data points are in the disordered phases with dense overlayers and especially low mobilities compared to other data points in the more ordered phases with higher area fractions (e.g., the violet circular, red circular, green triangular, and black triangular data points).

6 Discussion

We study the quasi-2D ordering of gravitationally confined monodispersed colloidal systems with various concentrations and Péclet numbers of particles. We find that particles with different Péclet numbers display distinct quasi-2D ordering behaviors.

For the 'heavy' colloidal particles with a large Péclet number (i.e., $Pe = 24$), the gravitational force has more significant effect on the particle motion, and therefore the particles will be dominated by sedimentation and tend to form a gravitationally confined quasi-2D structure, as explained in Section 2.1. Agreeing with the predictions, the monotone trends of both the magnitude and phase angle of ψ_6 with respect to the area fraction in Figure 6 indicate that the sedimented base layers are more ordered for the higher area fractions. The most ordered phase can be found at the highest area fraction. In addition, Figure 10b and 10c suggest that the base layers become more ordered for the denser overlayers, as the particle mobility decreases (Figure 10a). Therefore, the presence of the overlayer in a sedimented colloidal system probably promotes the base layer ordering for particles with $Pe = 24$.

Meanwhile, for the 'light' particles with relatively small Péclet numbers (i.e., $Pe = 13$ and 14), the thermal fluctuation has more influence on the particle motion and the diffusion of particles along the vertical direction is nonnegligible. Therefore, it is less probable for the particles to form a monolayer merely under the confinement of gravity, and the stacking of overlayer particles will be essential for the formation and ordering of the base layer. In accordance with different dynamics, in contrast to particles with $Pe = 24$, particles with $Pe = 13$ and 14 display distinct base layer phase behaviors with respect to the area fraction and the overlayer density. Figure 7 and 8 imply that the base layers are not necessarily more ordered as the area fraction increases. The highly ordered phases can be found at both the highest and some intermediate area fractions. The irregular ordering behaviors of particles with smaller Péclet numbers with respect to the area fraction can be explained by the effects of the overlayer on the base layer particle mobility. Specifically, Figure 11a and 12a imply that the dense overlayer can

constrain the diffusion and rearrangements of particles in the base layer. Therefore, depending on the state of the 3D colloidal system as the sedimentation takes place, the base layer may be 'locked' in a disordered phase by the overlayer particles and thereby form a metastable glassy state. For instance, the orange circular and the blue triangular data points in Figure 12 represent two possible glassy phases in highly disordered states accompanied with dense overlayers and low mobilities, compared to other data points in the more ordered phases with higher area fractions.

Overall, our experiments suggest that the highly ordered phase of a gravitationally confined quasi-2D structure will most probably be found in a sedimented colloidal system of particles with a relatively large Péclet number at a high area fraction. Meanwhile, we find that the quasi-2D base layer in a concentrated sedimented system of particles with a small Péclet number may be trapped by the overlayer particles in a metastable glassy state.

The scope of this work can be expanded from several perspectives. First, the evolution of monolayer structures in the sedimented colloidal systems with respect to time can be investigated by observing the ordering of base layers after sedimenting for different spans of time. Although the area fraction and particle ordering (measured by median $|\psi_6|$) are relatively stable after $15 - 30$ minutes of sedimentation in our experiments, the study [10] indicates that monolayer structures may still undergo coarsening where the sizes of ordered domains are slowly increasing and the systems are not in true stable states. Therefore, by giving the colloidal suspensions longer sedimentation time, we can study the potential effects of coarsening on the ordering of the metastable monolayer structures. We can also conduct more experiments on particles with different Péclet numbers within the range $Pe \in (14, 24)$ where a possible change in the quasi-2D ordering behaviors takes place. In addition, we can study the formation of the ordered quasi-2D structures, as well as that of the disordered glassy states, by recording and analyzing the sedimentation processes. Moreover, we are collaborating with Peiyao Wu and Dr. James Kindt at the chemistry department of Emory University who are working on the simulations of sedimented colloidal systems. We believe that the computational and experimental results

together will provide us with a better insight on the ordering of quasi-2D structures in the sedimented colloidal systems.

References

[1] V. J. Anderson and H. N. W. Lekkerkerker. Insights into phase transition kinetics from colloid science. *Nature*, 416:811–815, 2002.

[2] S. Auer and D. Frenkel. Suppression of crystal nucleation in polydisperse colloidals due to increase of the surface free energy. *Nature*, 413:711–713, 2001.

[3] E. P. Bernard and W. Krauth. Two-step melting in two dimensions: First-order liquid-hexatic transition. *Phys. Rev. Lett.*, 107:155704, 2011.

[4] J. C. Crocker and D. G. Grier. Methods of digital video microscopy for colloidal studies. *J. Colloid Interface Sci.*, 179:298–310, 1996.

[5] S. Dorosz and T. Schilling. On the influence of a patterned substrate on crystallization in suspensions of hard spheres. *J. Chem. Phys.*, 136:1–5, 2012.

[6] A. Einstein. On the movement of small particles suspended in a stationary liquid demanded by the molecular-kinetic theory of heat. *Annalen der Physik (Leipzig)*, 17:549–560, 1905.

[7] U. Gasser, Eric R. Weeks, Andrew Schofield, P. N. Pusey, and D. A. Weitz. Real-space imaging of nucleation and growth in colloidal crystallization. *Science*, 292:258–262, 2001.

[8] P. Habdas and E. R. Weeks. Video microscopy of colloidal suspensions and colloidal crystals. *Curr. Op. Coll. Int. Sci.*, 7:196–203, 2002.

[9] A. Kohler. New method of illumination for photomicrographical purposes. *J. Royal Microscopical Soc.*, 14:261–262, 1894.

[10] François A. Lavergne, Dirk G. A. L. Aarts, and Roel P. A. Dullens. Anomalous grain growth in a polycrystalline monolayer of colloidal hard spheres. *Phys. Rev. X*, 7:041064, 2017.

[11] I. N. Levine. *Physical Chemistry (5th Edition)*. McGraw-Hill, Boston, MA, 2002.

[12] B. Li, D. Zhou, and Y. Han. Assembly and phase transitions of colloidal crystals. *Nat. Rev. Mat.*, 1:15011, 2016.

[13] M. Marechal, M. Hermes, and M. Dijkstra. Stacking in sediments of colloidal hard spheres. *J. Chem. Phys.*, 135:034510, 2011.

[14] Thomas Palberg. Crystallization kinetics of colloidal model suspensions: recent achievements and new perspectives. *J. Phys.:Cond. Mat.*, 26:333101, 2014.

[15] Pawel Pieranski. Colloidal crystals. *Contemporary Physics*, 24:25–73, 1983.

[16] P. Pusey. *Liquids, Freezing and Glass Transition*. North-Holland, Amsterdam, 1991.

[17] P. Schall, D. A. Weitz, and F. Spaepen. Structural rearrangements that govern flow in colloidal glasses. *Science*, 318:1895–1899, 2017.

[18] E. R. Weeks. Introduction to the colloidal glass transition. *ACS Macro Lett.*, 6:27–34, 2017.